



CHORUS

This is the accepted manuscript made available via CHORUS. The article has been published as:

Barrier Crossing in Escherichia coli Chemotaxis

Zhaojun Li, Qiuxian Cai, Xuanqi Zhang, Guangwei Si, Qi Ouyang, Chunxiong Luo, and
Yuhai Tu

Phys. Rev. Lett. **118**, 098101 — Published 28 February 2017

DOI: [10.1103/PhysRevLett.118.098101](https://doi.org/10.1103/PhysRevLett.118.098101)

Barrier-crossing in *Escherichia coli* chemotaxis

Zhaojun Li,¹ Qiuxian Cai,¹ Xuanqi Zhang,¹ Guangwei Si,¹ Qi Ouyang,^{1,2,3} Chunxiong Luo,^{1,3,*} and Yuhai Tu^{1,4,†}

¹Center for Quantitative Biology, Academy for Advanced Interdisciplinary Studies, Peking University, Beijing, 100871, China

²Center for Quantitative Biology, Peking-Tsinghua Center for Life Science, Peking University, Beijing, 100871, China

³The State Key Laboratory for Artificial Microstructures and Mesoscopic Physics,

School of Physics, Peking University, Beijing, 100871, China

⁴T.J. Watson Research Center, IBM, P.O.Box 218, Yorktown Heights, New York 10598, USA

We study cell navigation in spatiotemporally complex environments by developing a microfluidic race-track device that creates traveling wave with multiple peaks and a tunable wave speed. We found that while the population-averaged chemotaxis drift speed increases with wave speed for low wave speed, it decreases sharply for high wave speed. This reversed dependence of population-averaged chemotaxis drift speed on wave speed is caused by a “barrier-crossing” phenomenon, where a cell hops backwards from one peak attractant location to the peak behind by crossing an unfavorable (barrier) region with low attractant concentrations. By using a coarse-grained model of chemotaxis, we map bacterial motility in an attractant field to random motion of an over-damped particle in an effective potential. The observed “barrier-crossing” phenomenon of living cells and its dependence on spatiotemporal profile of attractant concentration are explained quantitatively by Kramers reaction rate theory.

Sensing and responding to changes in external environments are critical for the survival of organisms. One of the well-studied model systems is bacterial chemotaxis. Bacteria use their transmembrane chemoreceptors to sense their environments and control their motion in search of places with more favorable conditions [1–3]. In a homogeneous environment, an *E. coli* cell performs the run-and-tumble random walk allowing it to explore its environment [4]. In the presence of an attractant gradient, *E. coli* cells bias their random walk towards the preferred direction by lengthening (shortening) the run time in the “correct” (“wrong”) direction. The intracellular biochemical circuit that allows an *E. coli* cell to compute gradient has been studied extensively in the past decades [5–9]. Predictive models have been developed based on knowledge of the bacterial signaling pathway and quantitative molecular and cellular experiments [10–13]. A modeling framework based on the intracellular signaling dynamics and the motor response has also been developed to study cellular and population behaviors [14–17].

However, cells live in heterogeneous environments together with other cells. There can be multiple favorable locations that are separated by unfavorable regions. Cells can also emit chemical signals and act as moving sources of attractants. Can a cell find its way out of a local optimum location to explore the environment globally? Can a cell track a moving attractant source? Here, we investigate these questions by developing a microfluidic device to create environments with multiple attractant peaks that move with a tunable speed. In particular, we created a traveling wave of attractant concentration in an annulus (race-track) channel as shown in Fig.1. Both population level behaviors and individual cell trajectories were measured for traveling wave attractant profiles with different wave speeds (v_w). Our measurements showed

that the population-averaged chemotaxis drift speed (v_d) increases with v_w for small v_w . Surprisingly, we observed a critical wave speed, beyond which v_d decreases sharply with v_w instead of reaching a saturating value. Our individual cell trajectory data revealed that cells can hop from one peak attractant position to another by crossing a barrier region with lower attractant concentrations, and the backward hopping probability increases with v_w .

To explain the experimental observations quantitatively, we studied a theoretical model of chemotaxis motion based on the intracellular signaling dynamics. Our model analysis showed that *E. coli* chemotactic behavior can be mapped to a thermally activated motion in an effective energy landscape, with the cells random motion acting as the source of thermal fluctuation and an effective potential determined by the ligand concentration profile. The effective potential barrier height for backward hopping is lowered by v_w , which results to a backward drift speed that depends exponentially on v_w . This exponential backward drift speed leads to the sharp drop in v_d at high v_w . Finally, the barrier-crossing phenomenon is confirmed by a “double well” experiment with different barrier heights..

We first describe our microfluidic device shown in Fig.1(a). The device is composed of concentration modulating parts, an annular observation channel, two agarose adding channels, and a cell loading channel. Attractant and buffer solutions, after being well mixed in the modulating parts, are pumped into the modulating parts with time varying injection speed. Details of the observation channel are presented in Fig.1(b). The connection channels between observation channel and source channels are filled with agarose gel and serve as control points. The hydrogel added from the agarose inlets is used to prevent bacteria escaping and avoid net flow that affects bacterial motility. The attractant concentration profile in the ob-

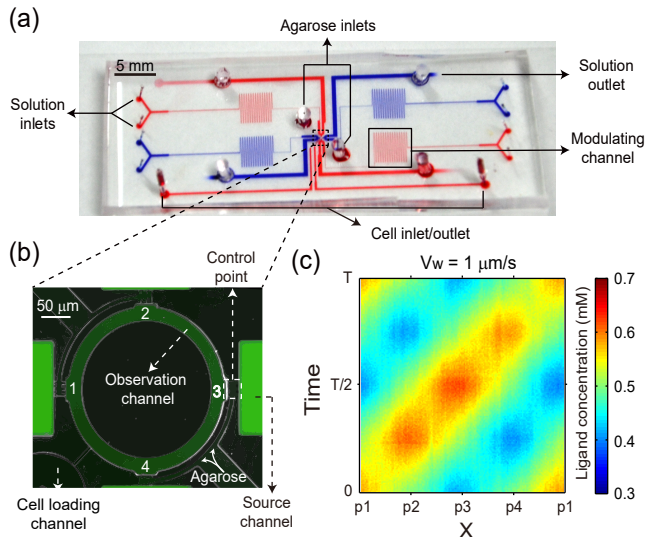


FIG. 1. Experiment setup. (a) The panorama of PDMS chip. (b) The zoomed-in picture of the observation channel. The circumference of the observation channel is $\lambda = 800 \mu\text{m}$. (c) The spatiotemporal profile of attractant (MeAsp) concentration in the observation channel for $v_w = 1 \mu\text{m/s}$. T represents the period of the concentration wave and p1-p4 are corresponding control points shown in (b). Attractant concentrations at the four source channels oscillate between 0 and 1 mM with a phase delay of $\pi/2$ in every two adjacent control points. The ligand concentration is measured by adding a small amount of fluorescein into attractant stocks.

ervation channel is determined by diffusion through the four control points. The same oscillation of attractant concentration (amplitude and period) was introduced in the four source channels with a phase delay of $\pi/2$ between two adjacent control points. As a result, the attractant molecules diffuse into the annular channel, forming a traveling-wave concentration field. The wave speed v_w is determined by the driving attractant period at the four control points. We test the attractant concentration in the observation channel by adding fluorescein in the attractant solution and the spatiotemporal concentration profile is shown in Fig.1(c) for $v_w = 1 \mu\text{m/s}$. The cell loading channel and observation channel are linked by a narrow pass. Because the attractant concentration in the observation channel is always higher than that in the loading channel during experiments, cells that are loaded to the cell loading channel can chemotax to the observation channel through the narrow pass and seldom escape out of it. [see supplementary material (SM) for detail of chip layout and fabrication].

Bacterial motion in the observation channel were imaged by using dark field lens. *E.coli* (wild type RP437) swimming in the traveling attractant wave (α -methyl-*DL*-aspartate (MeAsp)) with different wave speeds (v_w) 0.67 $\mu\text{m/s}$, 1 $\mu\text{m/s}$, 2 $\mu\text{m/s}$, 4 $\mu\text{m/s}$, 8 $\mu\text{m/s}$, 10 $\mu\text{m/s}$, 13.3 $\mu\text{m/s}$, are tracked and analyzed [see SM for details

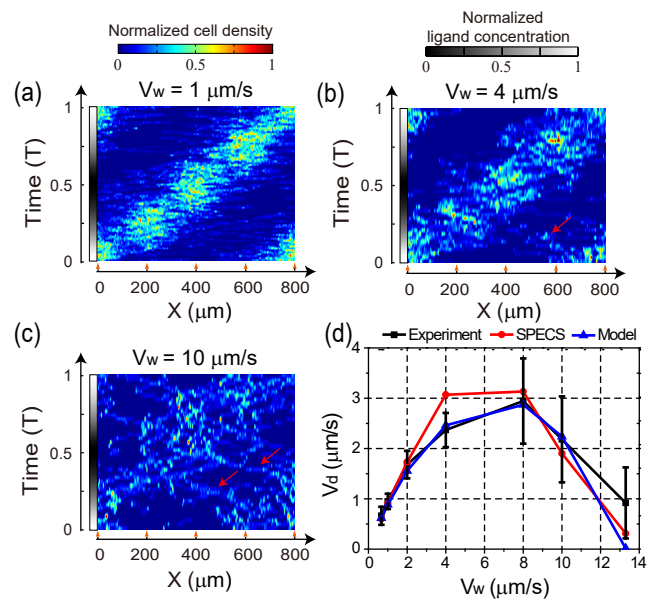


FIG. 2. Dynamics of bacterial population. The spatiotemporal cell density profiles for different wave speeds 1 $\mu\text{m/s}$ (a), 4 $\mu\text{m/s}$ (b), and 10 $\mu\text{m/s}$ (c). The normalized cell density and attractant concentration is represented by the color and gray scales respectively. The gray scale stripe on the left side of each panel shows the normalized ligand concentrations at $x=0$. The red arrows indicate the “backward” bacterial flux moving in the opposite direction of the attractant wave. (d) The bacterial drift velocity (v_d) averaged over a period versus v_w from experiments (black), SPECS simulations (red) and fitting with the Eq.4 and Eq. S26 (blue). The error bars denote standard deviation in 9 independent experiments.

of experiments]. The spatiotemporal cell density profiles for different wave speeds are shown in Figs.2(a)-(c). The bacterial chemotactic behavior depends strongly on v_w . For smaller $v_w \leq 4 \mu\text{m/s}$, most bacteria form a cluster following the crest of the attractant wave [Fig.2(a)-(b)]. Occasionally, a cell escapes from the cluster and moves in a backward direction opposite to the attractant wave as indicated by the red arrow in Fig.2(b). However, for higher $v_w > 4 \mu\text{m/s}$, such backward motion becomes more frequent leading to a more diffused cell distribution [Fig.2(c)].

To characterize the bacterial population dynamics at different v_w quantitatively, we calculated the bacterial drift velocity v_d by averaging the velocities of all cell trajectories within a period [see SM for details for trajectory extraction]. As shown in Fig. 2(d), for small wave speed $v_w \leq 2 \mu\text{m/s}$, we have $v_d \approx v_w$ as cells can follow the attractant wave. For intermediate $8 \mu\text{m/s} > v_w > 2 \mu\text{m/s}$, v_d starts to deviate from v_w but still increases with v_w albeit sub-linearly. This slowing down is likely caused by the effect of a finite adaptation time of *E. coli* in tracking/computing the attractant gradient [15, 16]. However, the most surprising observation is that v_d decrease

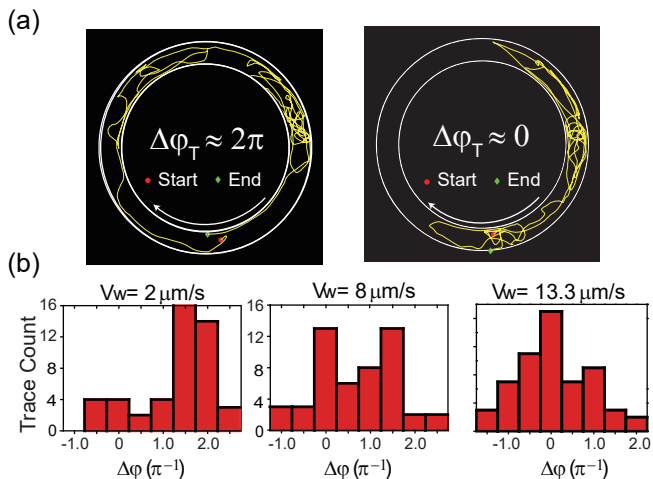


FIG. 3. Single cell dynamics. (a) Two representative single-cell trajectories with $\Delta\varphi_T \approx 2\pi$ (left panel) and $\Delta\varphi_T \approx 0$ (right panel) from experiment with $v_w = 8 \mu\text{m/s}$. The arrow shows the direction of attractant wave. (b) The statistics of $\Delta\varphi_T$ for $v_w = 2 \mu\text{m/s}$ (47 cells), $v_w = 8 \mu\text{m/s}$ (50 cells), and $v_w = 13.3 \mu\text{m/s}$ (51 cells).

sharply with v_w instead of saturating to a constant value when $v_w \geq 8 \mu\text{m/s}$. In the rest of this paper, we try to understand the observed non-monotonic dependence of v_d on v_w , in particular the sharp decrease in v_d for large v_w .

To characterize the relative motion of individual cells with respect to the traveling wave, we define the phase shift of a cell for a given period as $\Delta\varphi_T \equiv 2\pi\Delta x/(v_w T)$, where Δx is the net displacement along the direction of the attractant wave in a period T . If a cell follows the wave exactly, we have $\Delta\varphi_T = 2\pi$. If a cell hops backwards to the peak behind the current one during time T , we have zero net displacement $\Delta x = 0$, and $\Delta\varphi_T = 0$. Two representative trajectories for $\Delta\varphi_T \approx 2\pi$ and 0 are shown in Fig.3(a). Individual cell behaviors are analyzed by manually tracking their trajectories over a complete period. Fig. 3(b) shows the probability distributions of $\Delta\varphi_T$ for $v_w = 2 \mu\text{m/s}$, $8 \mu\text{m/s}$, and $13.3 \mu\text{m/s}$. For $v_w = 2 \mu\text{m/s}$, the $\Delta\varphi_T$ distribution peaks around a large $\Delta\varphi_T \sim 1.5\pi$. However, for $v_w = 8 \mu\text{m/s}$, an additional peak appears in the $\Delta\varphi_T$ distribution near $\Delta\varphi_T \sim 0$, indicating the significance of backward hopping, which is responsible for the significant reduction in v_d for large v_w . For the high wave speed $v_w = 13.3 \mu\text{m/s}$, the distribution is centered around $\Delta\varphi_T = 0$, which means backward hops dominate and the mean drift speed vanishes.

To understand both the population-level and individual cell behaviors quantitatively, we used the signaling pathway-based *E. coli* chemotaxis simulator (SPECS) [18] instead of the filter-function based phenomenological models[19–21]. The advantage of SPECS is that it incorporates the internal signaling pathway dynam-

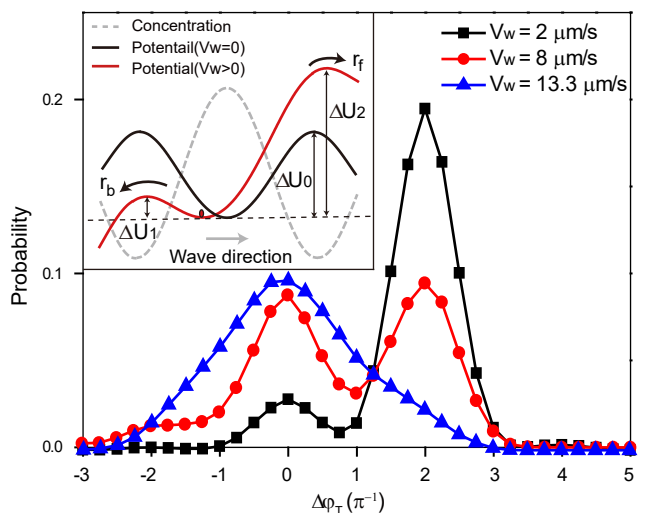


FIG. 4. The statistic of $\Delta\varphi_T$ for different wave speed from SPECS. The multimodality of density probability is caused by the “barrier-crossing” between the neighboring local well. The effective potentials for $v_w = 0$ and $v_w > 0$, and the attractant concentration profile are shown in the inset.

ics with the movements of individual cells (see SM for details of SPECS simulation). The dependence of v_d on v_w from SPECS agrees with our experimental data [Fig.2(d)]. We also studied statistics of $\Delta\varphi_T$ of individual cells for different traveling attractant wave speeds in SPECS. As shown in Fig.4, the $\Delta\varphi_T$ distributions exhibit multimodality with peaks centered around 2π and 0, and the proportions of bacteria distributed around different peaks change significant with v_w . For $v_w = 2 \mu\text{m/s}$, a large proportion of cells have $\Delta\varphi_T$ around 2π and only about $< 20\%$ of the population distributes near 0. As v_w increases, the proportion of the cells with $\Delta\varphi_T \sim 0$ increases, and eventually dominates at high v_w , which agrees with the experiments (Fig. 3(b)).

In our previous work, a mean field theory based on intracellular signaling dynamics was developed for studying population level bacterial chemotaxis behaviors [15, 17]. Briefly, the tumbling rate $z_t = \tau^{-1}(a/a_0)^H$ is modulated by chemoreceptors activity a , where τ and a_0 are the average run time and activity of chemoreceptors at steady state, $H(\approx 10)$ is the Hill coefficient [22]. The total frequency of a cell changing its direction is the sum of the rotational diffusion coefficient (z_0) and the tumbling rate (z_t): $z(a) = z_t + z_0$. Thus, the average run time is $\bar{z}^{-1} \approx z^{-1}|_{(a=\bar{a})}$ with \bar{a} the average activity of all cells at position x , and the average run distance is $v\bar{z}^{-1}$ with v the run speed. The dynamics of the receptor activity is governed by the local attractant concentration and the receptor methylation level, which has a slow dynamics and essentially carries a memory of the cells environment in the past. Therefore, when cells move in a chemical gradient, the average activity of the left-moving cells at

position x is different from the right-moving cells at the same position, as these two populations carry different receptor methylation levels. The activity difference leads to a difference in the tumbling frequency Δz , which eventually drives the bacterial chemotactic drift.

In our experiments with traveling attractant waves, it is convenient to study the system in a co-moving frame with the attractant by using the transformation $x' = x - v_w t$. The dynamics of the bacterial density $\rho(x', t)$ in the moving frame is given by:

$$\frac{\partial \rho}{\partial t} = \frac{\partial}{\partial x'} [D(x')U'(x')\rho] + \frac{\partial}{\partial x'} \left[D(x') \frac{\partial \rho}{\partial x'} \right], \quad (1)$$

which describes bacterial chemotaxis motility as the thermal motion of particles moving in an external potential [23]. The attractant field gives rise to the external potential and the bacterial random walk acts as the thermal fluctuation. As shown in details in SM, the diffusion coefficient $D(x')$ and the effective potential $U(x')$ can be expressed as:

$$D(x') \approx \frac{v^2}{\bar{z}} \left(1 + \frac{v_w \Delta z}{v \bar{z}} \right),$$

$$U(x') \approx \int_0^{x'} \frac{1}{D(x'')} \left(v_w + \frac{v \Delta z}{\bar{z}} \right) dx''. \quad (2)$$

The effective potential $U(x')$ given above by Eq. 2 depends on the wave speed v_w . The potential contributed by the attractant profile alone (i.e., $v_w = 0$) is periodic (black curve in Fig.4 inset). The effect of v_w is to tilt this periodic potential along the wave direction (x) to form a tilted washboard potential for $v_w > 0$ (red curve in Fig.4 inset). This can be seen by approximating D as a constant in Eq. 2, which leads to a term $v_w x'/D$ for the potential $U(x')$. In this washboard potential, a cell quickly moves to its closest well and stay there until the random walk motion drives it over a barrier into a neighboring well. Based on the classical Kramers theory of energy barrier crossing [24], the hopping rates along (forward) or against (backward) the attractant wave direction (r_f or r_b) depends on the barrier height (ΔU_1 or ΔU_2 , see Fig. 4 inset) exponentially:

$$r_b = r_0 e^{-\Delta U_1} \approx \alpha e^{\beta_1 v_w}, \quad r_f = r_0 e^{-\Delta U_2} \approx \alpha e^{-\beta_2 v_w}, \quad (3)$$

where r_0 is the base attempt rate, and α is the hopping rate for stationary wave. The constants β_1, β_2 are independent of v_w (see SM for detailed derivations). The discrete hopping events from one well to another explain the multimodality of the probability distribution of $\Delta \varphi_T$ [Fig. 3(b) and Fig. 4]. As v_w increases, the backward hopping rate r_b increases and the percentage of cells with $\Delta \varphi_T = 0$ increases. Put together, v_d is given by:

$$v_d = v_w - \lambda(r_b - r_f) \approx v_w - \alpha \lambda [e^{\beta_1 v_w} - e^{-\beta_2 v_w}], \quad (4)$$

where $\lambda = 800 \mu m$ is the peak-to-peak distance of the traveling wave. For small v_w , the hopping rates are small,

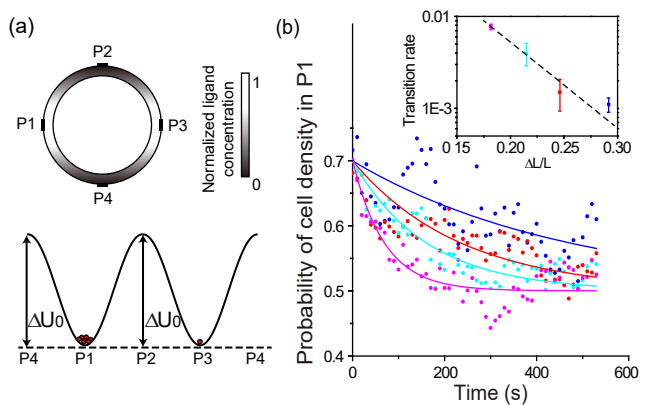


FIG. 5. Bacterial motion in a “double well potential”. (a) The concentration profile for generating a stationary “double well potential”. By controlling the attractant concentration difference between P1(P3) and P2(P4), we can control the barrier height. (b) Cells were concentrated around P1 initially. The cell population around P1 decays with time by escaping to P3. Inset shows the dependence of transition rates on the relative gradient, the dashed line indicates the predicted dependence (see Eq. S27 in SM).

so $v_d \approx v_w$. However, due to the exponential dependence of r_b on v_w , there exists a critical wave speed (v_c) where $dv_d/dv_w = 0$, and the drift velocity is dominated by the backward hopping term r_b and decreases sharply for $v_w > v_c$. In our experiments, the attractant wave amplitude had a weak dependence on v_w , which leads to $\alpha = \alpha_0(v_w/v)^d$, where $d \approx 1.34$ is determined from experiments, and α_0 is a v_w -independent constant (see SM for details). Quantitatively, Eq. 4 fits the experiments and SPECS simulations well with $\alpha_0 = 0.0141/s$, $\beta_1 = 0.0713 s/\mu m$ and $\beta_2 = 0.4915 s/\mu m$ as shown in Fig.2(d). Note that for a high wave speed $v_w = 13.3 \mu m/s$ Eq. 4 needs to be modified to include higher order terms (see Eq. S26 in SM).

To verify the barrier crossing effect, we studied chemotaxis in a “double well potential”. The double well potential is achieved in the same device by giving a static high concentration at control points P1 and P3; and a static low concentration at P2 and P4. Cells were concentrated initially near P1 by lowering the concentration at P3. Once a majority cell population is established around P1, the concentration at P3 is raised to form the double well potential [Fig.5(a)]. The cells hop probabilistically between P1 and P3, causing cell density in P1 to decay exponentially to 0.5 over time [Fig.5(b)]. When we increase the potential barrier by decreasing the concentration at P2 and P4, the decay rate decreases as expected from the transition state theory [Fig.5(b) inset].

In summary, by developing a “racetrack” microfluidic device we investigate bacterial chemotaxis behaviors in response to traveling attractant waves. The underlying mechanism is understood by a computational model

based on realistic signaling pathway dynamics. We believe that this combined approach, i.e., quantitative microfluidics experiments together with predictive models based on realistic signaling dynamics, can be extended to study other interesting biological phenomena, such as collective behaviors due to cell-cell communication through chemical signaling[25–28].

This work is partially supported by the National Natural Science Foundation of China (11434001). The work by YT is supported by NIH GM081747.

* pkuluocx@pku.edu.cn

† yuhai@us.ibm.com

- [1] H. C. Berg, *Physics Today* **5**, 53 (2005).
- [2] D. Kentner and V. Sourjik, *Current opinion in microbiology* **9**, 619 (2006).
- [3] S. L. Porter, G. H. Wadhams, and J. P. Armitage, *Nature Reviews Microbiology* **9**, 153 (2011).
- [4] H. C. Berg, D. A. Brown, *et al.*, *Nature* **239**, 500 (1972).
- [5] U. Alon, M. G. Surette, N. Barkai, and S. Leibler, *Nature* **397**, 168 (1999).
- [6] V. Sourjik and H. C. Berg, *Proceedings of the National Academy of Sciences* **99**, 123 (2002).
- [7] T. S. Shimizu, Y. Tu, and H. C. Berg, *Molecular systems biology* **6**, 382 (2010).
- [8] J. Yuan, R. W. Branch, B. G. Hosu, and H. C. Berg, *Nature* **484**, 233 (2012).
- [9] V. Sourjik, *Trends in microbiology* **12**, 569 (2004).
- [10] Y. Tu, *Annual review of biophysics* **42**, 337 (2013).
- [11] T.-M. Yi, Y. Huang, M. I. Simon, and J. Doyle, *Proceedings of the National Academy of Sciences* **97**, 4649 (2000).
- [12] Y. Tu, T. S. Shimizu, and H. C. Berg, *Proceedings of the National Academy of Sciences* **105**, 14855 (2008).
- [13] J. E. Keymer, R. G. Endres, M. Skoge, Y. Meir, and N. S. Wingreen, *Proceedings of the National Academy of Sciences of the United States of America* **103**, 1786 (2006).
- [14] R. Erban and H. G. Othmer, *SIAM Journal on Applied Mathematics* **65**, 361 (2004).
- [15] G. Si, T. Wu, Q. Ouyang, and Y. Tu, *Physical review letters* **109**, 048101 (2012).
- [16] X. Zhu, G. Si, N. Deng, Q. Ouyang, T. Wu, Z. He, L. Jiang, C. Luo, and Y. Tu, *Physical review letters* **108**, 128101 (2012).
- [17] B. Hu and Y. Tu, *PLoS Comput Biol* **10**, e1003672 (2014).
- [18] L. Jiang, Q. Ouyang, and Y. Tu, *PLoS Comput Biol* **6**, e1000735 (2010).
- [19] P.-G. De Gennes, *European Biophysics Journal* **33**, 691 (2004).
- [20] D. A. Clark and L. C. Grant, *Proceedings of the National Academy of Sciences of the United States of America* **102**, 9150 (2005).
- [21] A. Celani and M. Vergassola, *Proceedings of the National Academy of Sciences* **107**, 1391 (2010).
- [22] P. Cluzel, M. Surette, and S. Leibler, *Science (New York, N.Y.)* **287**, 1652 (2000).
- [23] N. G. Van Kampen, *Stochastic processes in physics and chemistry*, Vol. 1 (Elsevier, 1992).
- [24] H. A. Kramers, *Physica* **7**, 284 (1940).
- [25] E. O. Budrene and H. C. Berg, (1991).
- [26] S. Park, P. M. Wolanin, E. A. Yuzbashyan, P. Silberzan, J. B. Stock, and R. H. Austin, *Science* **301**, 188 (2003).
- [27] T. Nakagaki, H. Yamada, and Á. Tóth, *Nature* **407**, 470 (2000).
- [28] F. J. Hol and C. Dekker, *Science* **346**, 1251821 (2014).
- [29] See Supplemental Material [url], which includes Refs. [30–35].
- [30] G. Si, W. Yang, S. Bi, C. Luo, and Q. Ouyang, *Lab on a Chip* **12**, 1389 (2012).
- [31] I. F. Sbalzarini and P. Koumoutsakos, *Journal of structural biology* **151**, 182 (2005).
- [32] D. Clausnitzer, O. Oleksiuk, L. Løvdok, V. Sourjik, and R. G. Endres, *PLoS Comput Biol* **6**, e1000784 (2010).
- [33] U. Alon, L. Camarena, M. G. Surette, B. A. y Arcas, Y. Liu, S. Leibler, and J. B. Stock, *The EMBO journal* **17**, 4238 (1998).
- [34] M. Molaei, M. Barry, R. Stocker, and J. Sheng, *Physical review letters* **113**, 068103 (2014).
- [35] B. Mello and Y. Tu, *Biophysical journal* **92**, 2329 (2007).